



# Plastic film based lightweight thruster driven by triboelectric nanogenerator for multi-purpose propulsion applications<sup>☆</sup>

Kai Han<sup>a,b,1</sup>, Jianjun Luo<sup>b,c,1</sup>, Jian Chen<sup>b,1</sup>, Yujin Liu<sup>a</sup>, Jinliang Li<sup>a</sup>, Zhong Lin Wang<sup>b,c,d,\*</sup>, Wenjie Mai<sup>a,b,\*\*</sup>

<sup>a</sup> Siyuan Laboratory, Guangdong Provincial Engineering Technology Research Center of Vacuum Coating Technologies and New Energy Materials, Department of Physics, Jinan University, Guangzhou, Guangdong 510632, PR China

<sup>b</sup> Beijing Institute of Nanoenergy and Nanosystems, Chinese Academy of Sciences, Beijing 101400, PR China

<sup>c</sup> School of Nanoscience and Technology, University of Chinese Academy of Sciences, Beijing 100049, PR China

<sup>d</sup> School of Material Science and Engineering, Georgia Institute of Technology, Atlanta, GA 30332-0245, USA

## ARTICLE INFO

### Keywords:

Electroaerodynamics  
Thruster  
Propulsion system  
Triboelectric nanogenerator  
High voltage

## ABSTRACT

Electroaerodynamics (EAD) force, produced by the collisions of moving ions with neutral molecules from air or other gases in a high-strength electric field, has been proven as an alternative method of great potential for propulsion without combustion emissions. Here, we demonstrate a simple and easily-fabricated plastic film based lightweight EAD thruster (5.44 mg), which can produce a high entrained airflow up to  $3.65 \text{ m s}^{-1}$  with a corresponding thrust force of 0.68 mN under the applied voltage of 8.5 kV. As a new and promising energy technology, triboelectric nanogenerator (TENG), has shown its natural advantage of high voltage output for high-strength electric field building in various applications. With proper circuits, different forms of EAD thrusters and TENG power were combined into different propulsion systems, which can successfully propel boats moving forward, micro aircrafts flying and the maglev state globe rotating, showing great prospects in multiple fields.

## 1. Introduction

Since the phenomenon of the ionic wind was discovered as long as several centuries ago [1], the relevant researches were gradually deepened in a more scientific way and the theory was developed from electroaerodynamics (EAD) to electrohydrodynamics (EHD) as the range of applicative fluids broadened [2–7]. By the collisions of moving charged particles with neutral molecules in a high-strength electric field, a thrust force in the opposite direction of motion is produced, accompanied by other phenomena [1–7]. Such technology possesses advantages of no moving parts, being nearly silent and no combustion emissions, which is eco-friendly and helpful to achieve the goal of carbon neutrality. Based on these, a variety of applications are developed from propulsion and flow control to thermal management and food drying [7–14].

By corona discharge in common insulating medium air, it is easy to obtain an ionic wind and a corresponding EAD thrust [6]. Since it was proposed as a promising way for propulsion even for a flying craft, a lot of attempts have been tried to realize it, such as the hexagonal lifter described by Naudin [15], a series of studies about the flying micro-robot made by Drew [16,17], and the recent successful flight of an aeroplane with solid-state propulsion achieved by Xu [18]. However, there is still a long way to obtain a high enough thrust-weight ratio device for practical use. In addition, the current study about the complete propulsion system is scarce, from the perspective of energy source and utilization. Thus, it is significant to keep developing lightweight and simple devices and introduce new energy technology for further enhancement of application value.

Triboelectric nanogenerator (TENG) [19], originating from the

<sup>☆</sup> Prof Zhong Lin Wang, an author on this paper, is the Editor-in-Chief of Nano Energy, but he had no involvement in the peer review process used to assess this work submitted to Nano Energy. This paper was assessed, and the corresponding peer review managed by Professor Chenguo Hu, also an Associate Editor in Nano Energy.

<sup>\*</sup> Corresponding authors at: Beijing Institute of Nanoenergy and Nanosystems, Chinese Academy of Sciences, Beijing 101400, PR China.

<sup>\*\*</sup> Corresponding authors at: Siyuan Laboratory, Guangdong Provincial Engineering Technology Research Center of Vacuum Coating Technologies and New Energy Materials, Department of Physics, Jinan University, Guangzhou, Guangdong 510632, PR China.

E-mail addresses: [zlwang@gatech.edu](mailto:zlwang@gatech.edu) (Z.L. Wang), [wenjiemai@email.jnu.edu.cn](mailto:wenjiemai@email.jnu.edu.cn) (W. Mai).

<sup>1</sup> These authors contributed equally to this work

Maxwell's displacement current [20,21], is a new and developing energy harvesting technology that can convert multiform mechanical energy into electric energy effectively for various applications [22–31]. One of its intrinsic property is high voltage output, by which a strong electric field can be easily created. Compared with traditional high-voltage power source, TENG is easily fabricated with simple structure, which makes it have advantages in portability and cost-effectiveness. Lots of reported applications have indicated that TENG can be used as an efficient high voltage supplier, such as electrostatic actuation [32], electron field emission [33], ion and plasma generation (including in a corona discharge way) [34–39]. Therefore, TENG will be a promising way to build a complete propulsion system with the EAD thruster.

In this work, by introducing a simple method to produce the plastic film based electrode component, we demonstrate an easy-fabricated lightweight EAD thruster. TENGs with four sizes of rotors were prepared to investigate their voltage output performance. Three kinds of methods based on different circuits were used to combine the TENG and the thruster into a complete propulsion system. With TENG-driven, EAD thrusters in different forms can effectively produce thrust to propel different kinds of devices, including foam boats, micro aircrafts and the maglev globe, showing great application potential in fields of water transport, aviation and space.

## 2. Experimental

### 2.1. Fabrication of EAD thrusters and measurements of entrained airflow speed

The plastic film, a kind of polyester (PET) release liner, is the leftover stripped from the polyimide (Kapton) tape when fabricating a TENG. Fig. S1 shows its Fourier transform infrared spectrum (iS20, Thermo Scientific Nicolet) with the standard spectrum. From the view of saving, it was reused as the substrate to prepare the collector electrode. The film was cut according to the designed patterns by a laser cutting machine (PLS6.75, Universal). The diameter of the outer edge is 11 mm, which is 1 mm wider than the core patterned region. Then, the patterned substrates were coated with a conducting layer of gold (Au) by a vacuum evaporation way (ZHD300, Technol) to form collector electrodes. The evaporation rate is  $0.2 \text{ A s}^{-1}$ , and the thickness of the Au layer is about 100 nm. Tungsten (W) wires with the length of 12 mm and different diameters (0.1 mm, 0.15 mm, and 0.25 mm) were used as emitter electrodes in the direction that is perpendicular to the collector electrode. After being installed in the airflow testing device, a high voltage power (DW-P303–1ACFD, Dong Wen High Voltage) was connected with two electrodes by enameled copper wire. The flow speed was tested by a hot wire anemometer (405i, Testo) with an app installed on a phone. To avoid the disturbance from the ambient environment, a cubic acrylic box (the side length is 36 cm) was used to cover the whole testing system in it. And the temperature and humidity in it were tested by a thermometer & humidity meter (DT-625, CEM) as shown in Fig. S2.

### 2.2. Fabrication of TENGs and measurements of electric performance

The rotor of the TENG is a 0.3 mm thick epoxy glass fiber (commonly named FR-4) disk board with four pieces of 60  $\mu\text{m}$  thick fan-shaped Kapton film stuck on it. The diameters of four rotors are 15 cm, 20 cm, 25 cm, 30 cm, and the area of Kapton films on them is 55  $\text{cm}^2$ , 113  $\text{cm}^2$ , 192  $\text{cm}^2$  and 290  $\text{cm}^2$ , respectively. The stator is a custom-made printed circuit board (PCB) with four pairs of copper (Cu) electrodes. A small vertical gap ( $< 0.5 \text{ mm}$ ) was set between the rotor and the stator. Artificial wool cloth was cut into a stipe with a width of 3 cm and stuck on a PMMA substrate to make a triboelectrification brush. After all components were assembled into a TENG, a direct current high-speed motor (895, Xiao Jiang) was selected as the simulated mechanical energy source. By adjusting the rotation speed, the basic performance was

measured by an electrometer (6514, Keithley) and a multimeter (P188, Pintech) with a high-voltage attenuation rod (1 G $\Omega$ , HVP-40, Pintech) and a bridge rectifier composed of four high-voltage diodes (20 kV).

### 2.3. Measurements of the propulsion system with TENG-driven in different methods

In Method-1, four high-voltage diodes (20 kV) were welded together as the bridge rectifier. In Method-2, one high-voltage diode and one high-voltage capacitor (20 kV, 10 nF) were welded as a unit. Different numbers of units were grouped into different voltage booster circuits. In Method-3, a two-unit voltage booster circuit was combined with a series of high-voltage resistors (RI80, 5 W, 15 kV). The same airflow testing device was used. The voltage in Method-2 was measured by the multimeter with a high-voltage attenuation rod of 1 G $\Omega$ . The voltage in Method-3 was calculated from the current, which was measured by the 6514 electrometer.

## 3. Results and discussion

### 3.1. Design and characterization of plastic-based lightweight EAD thrusters

Typically, a low diameter electrode (typically a wire or a needle) is used as the positive emitter [11], and a blunt electrode as the negative collector or counter to make up a EAD thruster. As an essential component, the collector electrode was prepared in a simple method as shown in Fig. 1a. Considering that plastic generally has low density, a piece of plastic film with a thickness of 80  $\mu\text{m}$  was used and processed by laser cutting according to the designed pattern. Then, by a vacuum evaporation method, the substrate with four pins was covered with a conducting layer forming the collector electrode. To ensure the stability of the electrode, corrosion-resistant Au was selected in this work. By adjusting the hole size of the pattern, a series of collector electrodes were prepared. Fig. 1b shows their pictures, including 6 circular meshed samples (named from M1 to M6) and a single ring sample (named S). The hole area of each sample is 31.3  $\text{mm}^2$  (M1), 45.5  $\text{mm}^2$  (M2), 53.3  $\text{mm}^2$  (M3), 55.7  $\text{mm}^2$  (M4), 58.7  $\text{mm}^2$  (M5), 58.8  $\text{mm}^2$  (M6), and 63.6  $\text{mm}^2$  (S), respectively. As for the emitter electrode, the W wire which has a high melting point was chosen as the material. A typical fabricated thruster device is shown in Fig. 1c. Fig. 1d illustrates the main producing process of the ionic wind and the following entrained airflow, which are caused by the positive corona discharge. When applying a high positive voltage, bipolar ions are generated in the corona plasma region at the tip of the emitter electrode. Under the action of the electric field, positive ions are accelerated and collide with neutral molecules, causing them to move to the collector electrode and through the mesh holes.

In order to investigate the performance of the fabricated EAD thruster, the entrained airflow speed was measured as a simple and direct characterization result. An airflow testing system was designed and constructed (Fig. 2a). The collector electrode is fixed in a clip consisting of two silicone sheets and two acrylic boards with same holes of 10 mm in diameter. And the emitter electrode is fixed in the midpoint of an acrylic cross on a short acrylic tube, which is stuck with one clip-board. A longer acrylic tube with an inner diameter of 10 mm stuck on the other clipboard is used as the flow channel, of which the cross-sectional area is 78.5  $\text{mm}^2$ . On the wall of the tube there are two drilled holes, in which a hot-wire anemometer is placed for airflow information acquisition. Fig. 2b shows the COMSOL simulation of the motion trajectories of charged particles in a cylindrical space with an applied voltage of 6.0 kV, indicating that the device will work properly. The simulation of the electric potential distribution of the thruster is shown in Fig. S3. To display the entrained airflow more intuitively, we made a smoke disturbance demonstration (Video S1). As shown in Fig. 2c, the existence of airflow can be clearly observed when the high voltage of 6.0 kV was applied on the thruster.

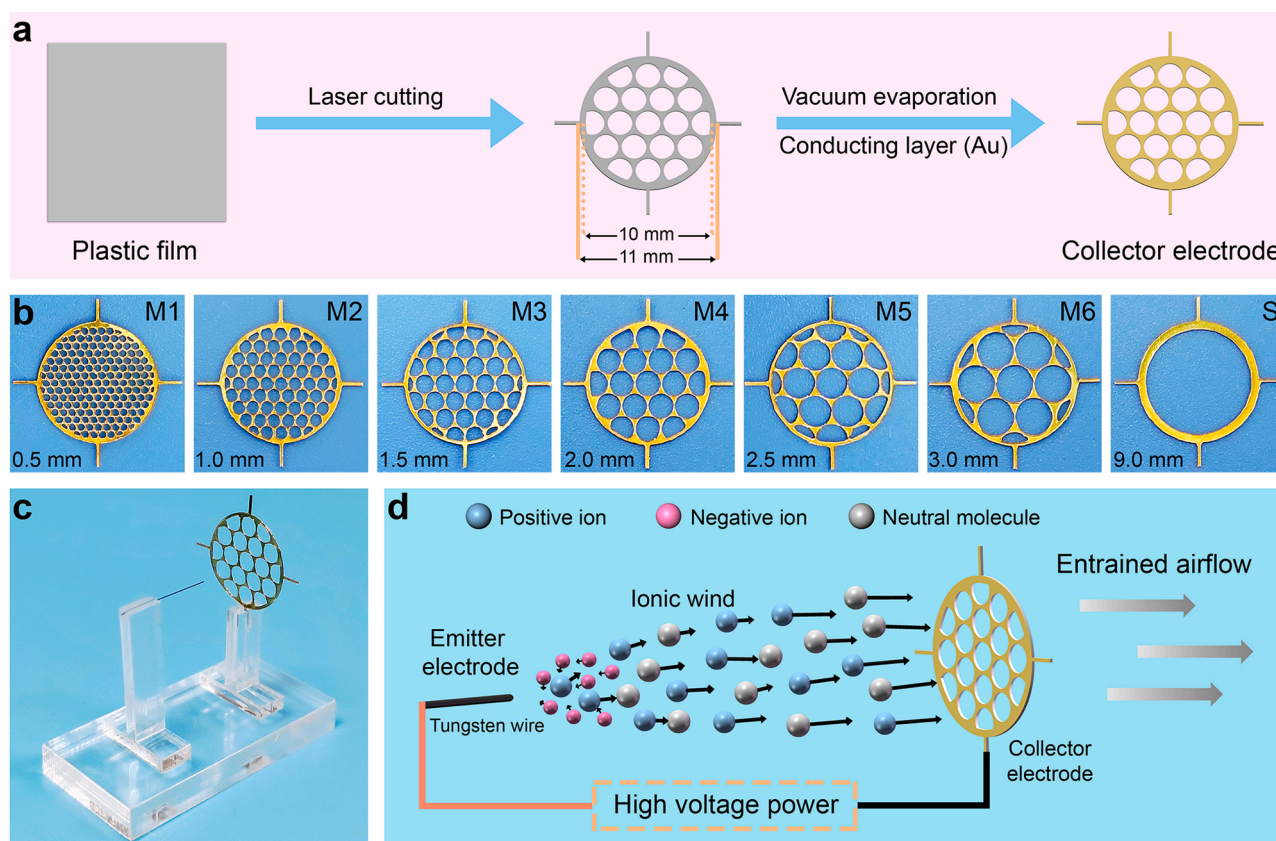


**Fig. 1.** Design and preparation of the EAD thruster. (a) Schematic diagram of the preparation process of the plastic film based collector electrode. (b) Photographs of collector electrodes with different circular meshes. (c) Photograph of a typical thruster placed on an acrylic display stand. (d) Schematic diagram of the working principle of the EAD thruster.

Supplementary material related to this article can be found online at [doi:10.1016/j.nanoen.2022.107558](https://doi.org/10.1016/j.nanoen.2022.107558).

Before systematic tests, W wires in three diameter sizes (0.1 mm, 0.15 mm, and 0.25 mm) were used to make different thrusters with the simple single ring collector electrode S for parameter optimization. As illustrated in Fig. S4, the smaller the diameter, the higher the airflow speed at the high voltage region, although the difference is not obvious. And the thruster with a smaller emitter electrode shows better response at the relatively low voltage region. However, a much thinner wire is too soft to operate. Therefore, the W wire with 0.1 mm in diameter was chosen as the emitter electrode for the following thruster fabrication and tests. The detailed testing information of all thrusters (named from T-M1 to T-M6 and T-S) is shown in Fig. 2d and Fig. S5. With the increase of the applied voltage, the airflow speed gradually increases. Meanwhile, we found that when the current between electrodes is less than 0.01 mA (the green dashed line region), the thruster worked normally in a safe state (Fig. S6). As the voltage increases, the current value rises up. While it exceeds 0.02 mA (the red dashed line region), the risk of discharge breakdown increases dramatically. Especially, at the interelectrode distance of 4 mm, the unwanted discharge breakdown occurred even below 0.02 mA. This kind of phenomenon was also observed for other thrusters (Fig. S7). Thus, there is a limit voltage range for each thruster at different interelectrode distances. As for the thruster T-M4, the usable applied voltage range is 3.0–8.5 kV under the optimal distance condition of 6 mm. Fig. 2e illustrates the statistic maximum average airflow speed results. As the hole diameter increases, the performance gets better from T-M1 to T-M4. This trend may be due to an increasing flow that passes through the holes. However, the process of the hole area enlarging will also be accompanied by the nonuniformity enhancement of the built-in electric field between the edge and the center, which may cause the performance degradation as T-M5 and T-M6 performed. All

hole meshed thrusters achieved their best performance under conditions of the interelectrode distance of 6 mm and the applied voltage of 8.0 or 8.5 kV. As for the thruster T-S, the optimum condition is 10 mm and 9.5 kV, which is inferred caused by its extreme nonuniformity of the built-in electric field. T-M4 has the best performance ( $3.65 \text{ m s}^{-1}$ ) of all thrusters, and Fig. 2f shows its measured airflow curve (the pink line) at the best condition. Based on the principle of interaction force, we made a simple calculation of the thrust force (the blue line) by using the Eq. (1).

$$F = 0.5\rho v^2 S \quad (1)$$

$\rho$  is the air density ( $1.293 \text{ kg m}^{-3}$ ),  $v$  represents the airflow speed, and  $S$  is the channel sectional area ( $78.5 \text{ mm}^2$ ). After calculation, the average thrust can achieve 0.68 mN. Based on the weight of T-M4 (5.44 mg), including the collector electrode (3.80 mg, Fig. S8a) and the emitter electrode (1.64 mg, Fig. S8b), the thrust weight ratio reached as high as 12.76. As a result, T-M4 was chosen as the basic thruster unit in the following research due to its excellent performance.

### 3.2. Performance of TENGs

Benefitting from its characteristic of high output voltage, TENG is very suitable for driving the EAD thruster. The non-contact-sliding freestanding mode was selected to construct a high-performance TENG [40], which can easily produce corona discharge with a proper discharge device [26]. Typically, it consists of a PCB stator and a FR-4 based rotor covering with Kapton film as the dielectric material (Fig. 3a). From the view of continuous high output and animal conservation, artificial wool was introduced to make the soft friction with Kapton film and supply sustained charges on the rotor surface [41]. Fig. S9 is the photograph of a typical TENG with an artificial wool brush.

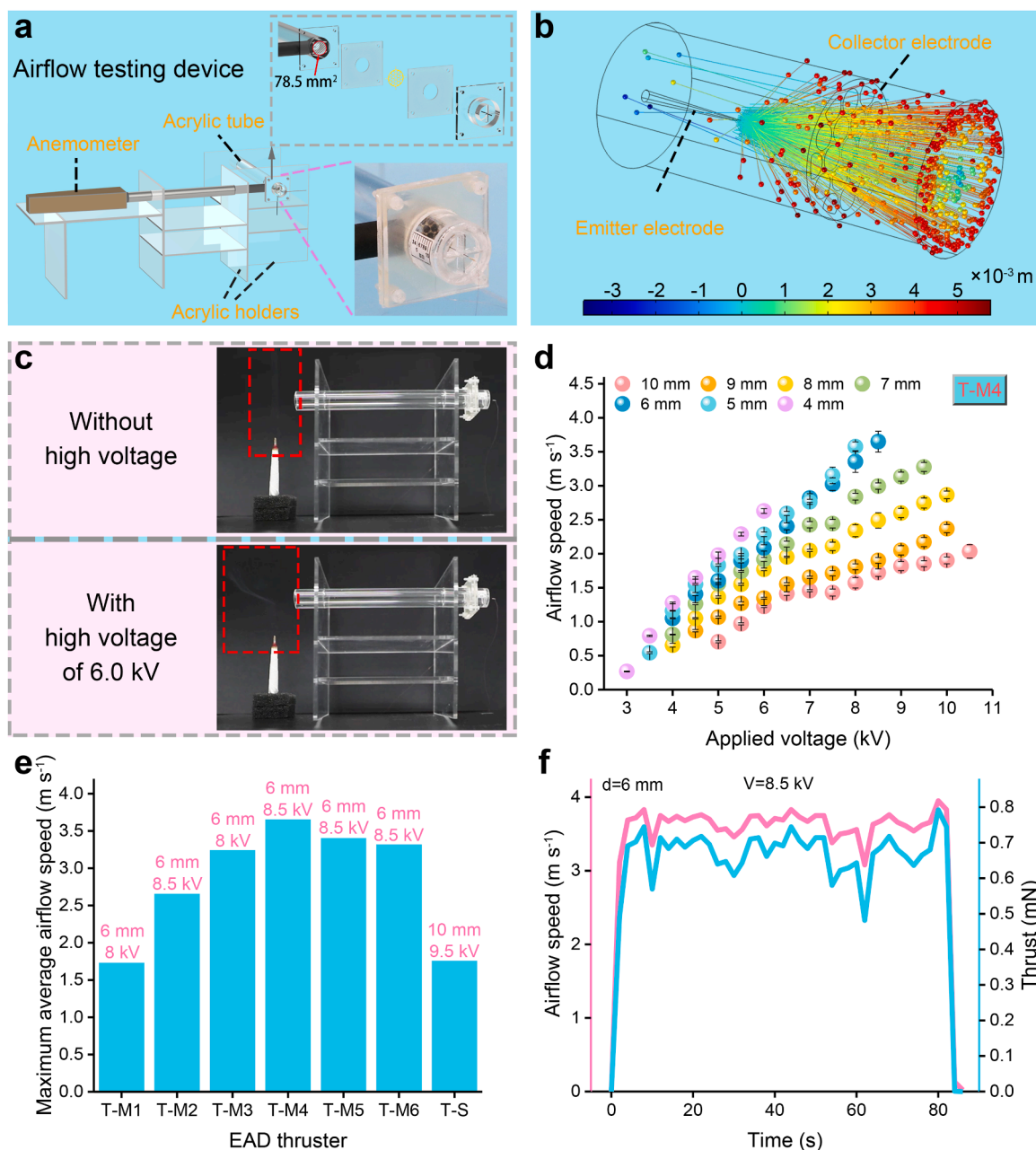


**Fig. 2.** Airflow speed tests under simulated conditions by a high voltage power supply. (a) Schematic diagram of the airflow testing device with photograph of the key testing component. (b) Simulation result of the motion trajectories of charged particles. (c) Screenshots of the smoke disturbance demonstration. (d) Airflow speeds of T-M4 under different interelectrode distances and applied voltages. (e) Maximum average airflow speed results of different thrusters. (f) Airflow speed and thrust curves of T-M4 under the interelectrode distance of 6 mm and the applied voltage of 8.5 kV.

The working principle of the TENG is illustrated in Fig. 3b. With the constant friction, the Kapton film is always negatively charged, positive charges are induced in the bottom electrode at the same time. During the first half cycle, as the rotor moves, the positive charges will flow to the next electrode in the circuit and produce a positive voltage until the Kapton film reaches the overlapping position. As it keeps moving, the induced positive charges continue to flow to the next electrode and produce a reverse voltage in the circuit. When the Kapton film and the electrode of next pair are overlapping, a complete electricity generation cycle is completed.

To avoid unnecessary waste, the same stator was combined with four rotors in different diameter sizes (15 cm, 20 cm, 25 cm and 30 cm) separately to fabricate different TENGs (TENG-15, TENG-20, TENG-25 and TENG-30) for their basic electrical performance investigation. A

motor was utilized to simulate the mechanical energy source and generate rotating power in a range of 1000–5000 RPM. As shown in Fig. 3c–f, with the increase of rotation speed up to 5000 RPM, the transferred charge of each TENG achieved 0.48  $\mu\text{C}$ , 0.97  $\mu\text{C}$ , 1.74  $\mu\text{C}$ , and 2.05  $\mu\text{C}$ , respectively. The voltage performance shows different ranges (2.1–2.5 kV, 3.6–4.4 kV, 6.4–7.8 kV, 7.6–8.6 kV), some of which are high enough to drive the thruster directly. Other basic performance results are illustrated in Fig. S10. As for the short-circuit current, TENGs can output as high as 0.25 mA, 0.50 mA, 0.87 mA, and 1.04 mA under the rotation speed of 5000 RPM. Based on the rectified current with a series of resistances in the circuit (Fig. S11), the maximum peak power reached 0.24 W, 0.72 W, 2.23 W, and 2.44 W, respectively. Additionally, as the diameter of rotors increases, the overall performance of TENGs shows an obvious increase. However, the capacity of the increase

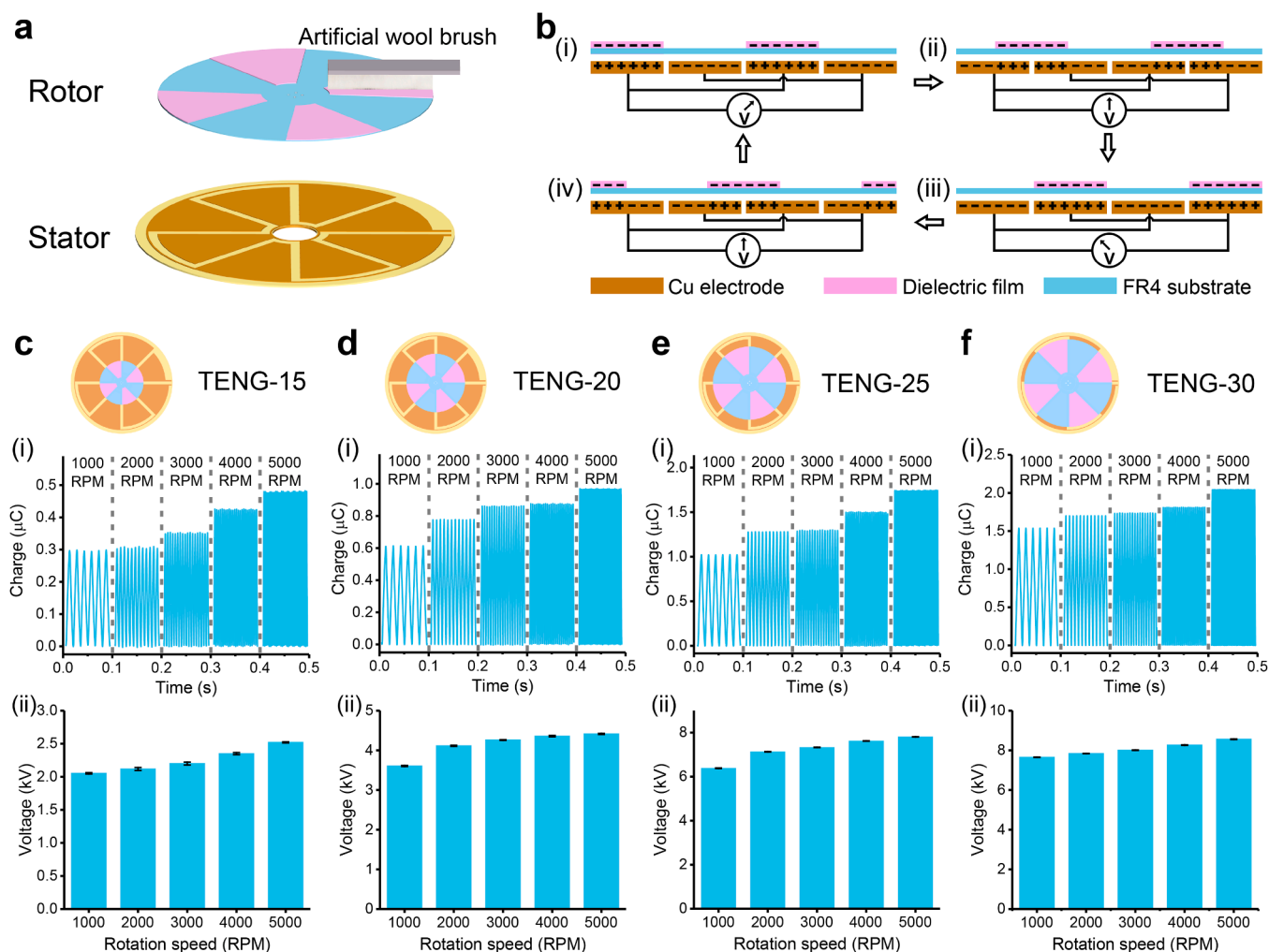


**Fig. 3.** Structure, working principle and performance of TENGs. (a) Schematic diagram of the structure of the disk TENG with an artificial wool brush. (b) Schematic diagram of the working principle of the TENG. (c–f) Performance of TENG-15, TENG-20, TENG-25, and TENG-30: (i) transferred charge and (ii) voltage tested by using a high-voltage attenuation rod of 1 GΩ after rectifying.

gradually weakens. It may be attributed to the unwanted frictions between the rotor and the stator, which are caused by the rotor's decreasing ability of keeping horizontal as the diameter increases. Apart from the electric performance, a simple abrasion test using the rotor of TENG-30 was done to detect the wear condition. As shown in Fig. S12, except a few unwanted frictions on the substrate due to the unsatisfactory flatness, there are no obvious plenty of new friction traces on the tribolayer after working at the speed of 5000 RPM for 1 h. On the whole, the fabricated TENGs can output high performance with durable working property, which creates possibilities for the effective drive to EAD thrusters.

### 3.3. TENG-driven propulsion system

Owing to its excellent electrical performance, TENGs can output high voltage that covers the usable applied voltage range of T-M4. Therefore, a direct drive method (Method-1) is first considered by a simple rectification (Fig. 4a). Directly driven by TENG-20, TENG-25 and TENG-30, the airflow speed results at an interelectrode distance of 6 mm are shown in Figs. 4b–d, separately. As for the TENG-15, no airflow was detected due to its low output voltage. In addition, another condition of 10 mm was also tested with the drive of TENG-30 (Fig. S13). These airflow speed results show a good correspondence with the output voltage of TENGs. It can be seen that the thruster exhibits a better performance with the increase of the rotation speed and the diameter of the

rotor. However, when the rotor of TENG-30 speeded up to 3000–5000 RPM, the discharge breakdown occurred because of the too high output voltage, indicating that the mechanical regulation way by changing the size of rotor or by adjusting the rotation speed has its limitation.

To overcome the problem of the low voltage, a series of voltage booster circuits with different numbers of units were utilized (Method-2, Fig. 4e), in which one unit consists of a high-voltage capacitor and a high-voltage diode. Fig. 4f shows the boosted voltage results of TENG-15 and TENG-20 under different rotation speeds with the unit number increasing. As marked in the red dash-dotted box, when the unit number is up to six and four, respectively, the two TENGs can output excessive voltage out of the usable range of T-M4. As for TENG-20 and TENG-30, a two-unit booster circuit is sufficient to meet the range because of their high original output (Fig. 4g). To verify the effect of voltage boosting, the TENG-15 with a six-unit booster circuit was tested. The airflow speed can be detected under the condition of 1000–3000 RPM and the discharge breakdown was observed when applying a higher speed (Fig. 4h), which has a good correspondence with the boosted voltage. This fully indicates that a low output TENG can reach the requirement to drive the EAD thruster with the method of voltage boosting.

Nevertheless, it should be noted that the voltage variation is still not continuous just by changing the booster unit number in a circuit. Therefore, a combined method (Method-3) by introducing a series of resistors to help regulate the output voltage was proposed as shown in Fig. 4i. The thruster is connected with resistors in parallel. Using TENG-

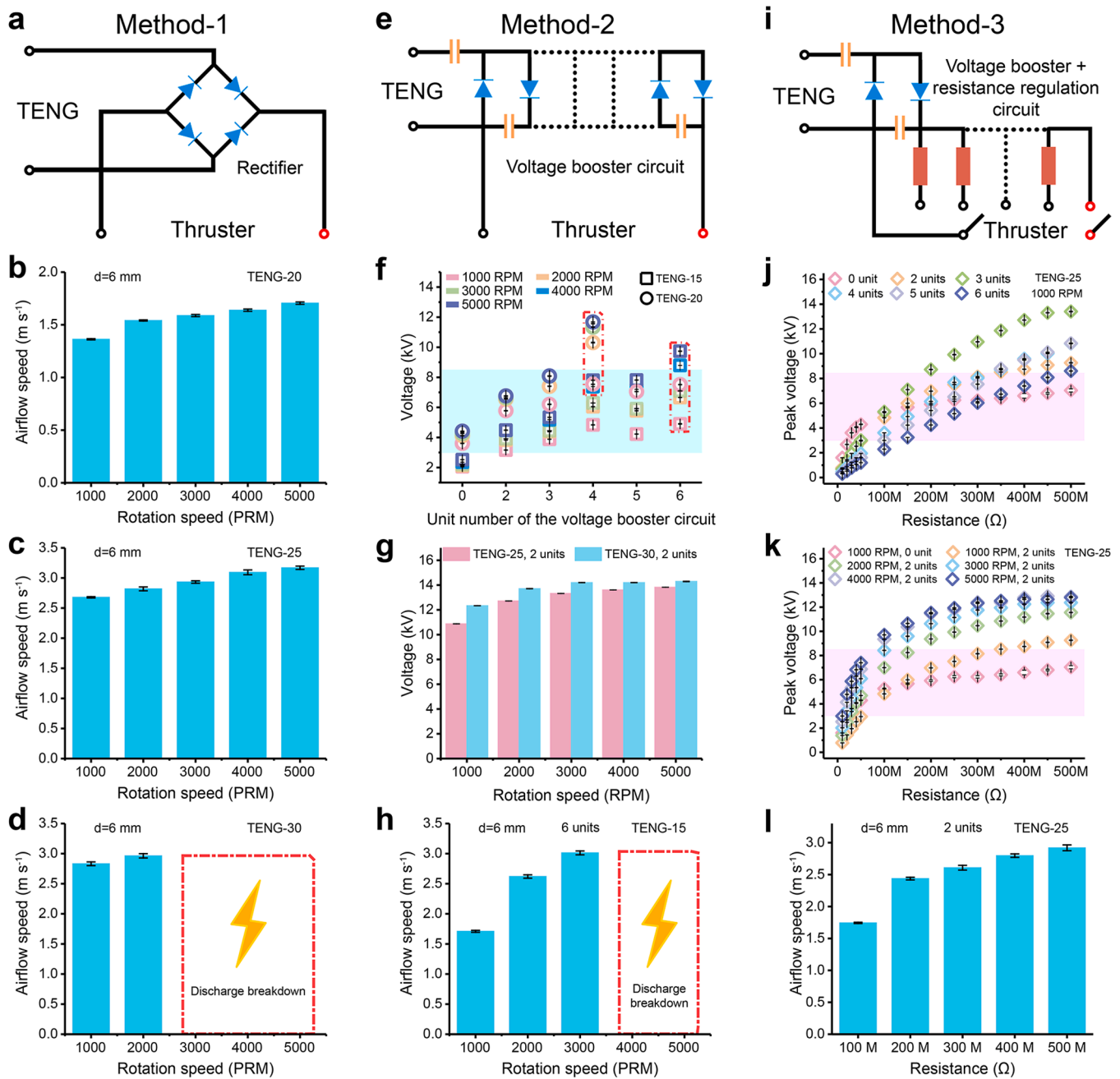


**Fig. 4.** Airflow speed tests with TENG-driven in different methods. (a) Schematic diagram of the TENG-driven propulsion system in Method-1. Airflow speed results under the drive of (b) TENG-20, (c) TENG-25, (d) TENG-30. (e) Schematic diagram of the TENG-driven propulsion system in Method-2. (f) Voltage results of TENG-15 and TENG-20 with a series of booster circuits. (g) Voltage results of TENG-25 and TENG-30 with a 2-unit booster circuit. (h) Airflow speed results under the drive of the boosted TENG-15. (i) Schematic diagram of the TENG-driven propulsion system in Method-3. (j) Peak voltage ( $I \times R$ ) across different resistors under the drive of the TENG-25 at a rotation speed of 1000 RPM with different booster circuits. (k) Peak voltage ( $I \times R$ ) across different resistors under the drive of the TENG-25 at different rotation speeds with a 2-unit booster circuit. (l) Airflow speed results under the drive of the TENG-25 with a 2-unit booster circuit and different resistors.

25 as the power source, we tested the current of the circuit with only loads of resistors first and calculated the voltage ( $I \times R$ ) to show a clearer character of the voltage variation trend. By changing the unit number of the voltage booster circuit, the statistical peak voltage data are shown in Fig. 4j. With the resistance increasing, the range of the output voltage is effectively extended, which covers the usable region easily. However, there is no distinct voltage change rule by modulating the booster unit. As for the condition of the solid unit number and different rotation speeds, it is clear to see a trend of overall increase of voltage and a trend of smaller resistance ranges available for the usable voltage region (Fig. 4k). Fig. S14 and Fig. S15 illustrate more details about the original

current and the calculated voltage by taking the booster unit and rotation speed as adjustment variables. Based on this method, the voltage applied can be regulated in a more controllable way. Fig. 4l and Fig. S16 show the results under different interelectrode distances by using the Method-3, indicating a good regulation effect for wider airflow speed and thrust ranges.

### 3.4. Demonstrations of multi-purpose applications

TENG is an efficient way to convert mechanical energy into electric energy, and the generated energy can be transferred into mechanical

thrust by utilizing the EAD thruster. Based on these, we first proposed a concept that combining these two technologies to help water transport with less carbon emission by using a series of TENGs and collecting the residual mechanical energy from the hydropower station (Fig. 5a). To verify its feasibility, a foam body and a EAD thruster were assembled into a boat (Fig. 5b). A plastic film shed was added to protect the thruster from water during the experiment. A commercial hydrophobic layer was sprayed on the bottom of the boat for less water resistance. The weight of the empty boat is 271.23 mg (Fig. S17a). In order to reduce the disturbance from the strong electrostatic attraction caused by high voltage, we simplified the testing system. A soft silver wire was used to connect the emitter electrode with the positive electrode. As for the collector electrode, the connected short wire was put into the water directly and the connection with the negative electrode is established by using water as the medium. A piece of copper wire mesh was also set up around the glass sink for electrostatic shielding. Under the direct drive of TENG-25 at the rotation speed of 1000 RPM, the empty boat headed to the opposite side quickly with the velocity of about  $3.4 \text{ cm s}^{-1}$  (Video S2).

Fig. 5c shows its initial state and motion state driven by the TENG after 3 s. To further show the transportation capacity, three 500 mg weights were loaded on the boat (Fig. 5d and Fig. S17b). The boat was driven with the same condition (Video S3) and the screenshots of two states are shown in Fig. 5e. The distance of the loaded boat moved is shorter with a velocity of  $1.4 \text{ cm s}^{-1}$ . Moreover, a management circuit from Method-3 was constructed to make a control of the navigation (Fig. S18). And we proposed a method to effectively avoid the over high voltage being applied on the thruster directly during the process of shifting resistor. The schematic diagram of working mechanism is shown in Fig. S19. By using different resistors (50 M $\Omega$ , 100 M $\Omega$ , 200 M $\Omega$ ), the boat moved with different velocities (Video S4). The counted data and screenshots of the motion state with TENG-driven after 6 s are shown in Fig. 5f. It is clear to see that the movement velocity of the boat increases with the increase of the resistance. To further demonstrate the application potential, we made a larger boat (7.455 g, Fig. S20) with thrusters in a single line array of 5 units (Fig. 5g) and drove the boat directly by TENG-25. The boat was put in a long plastic sink with two metal slide ways.

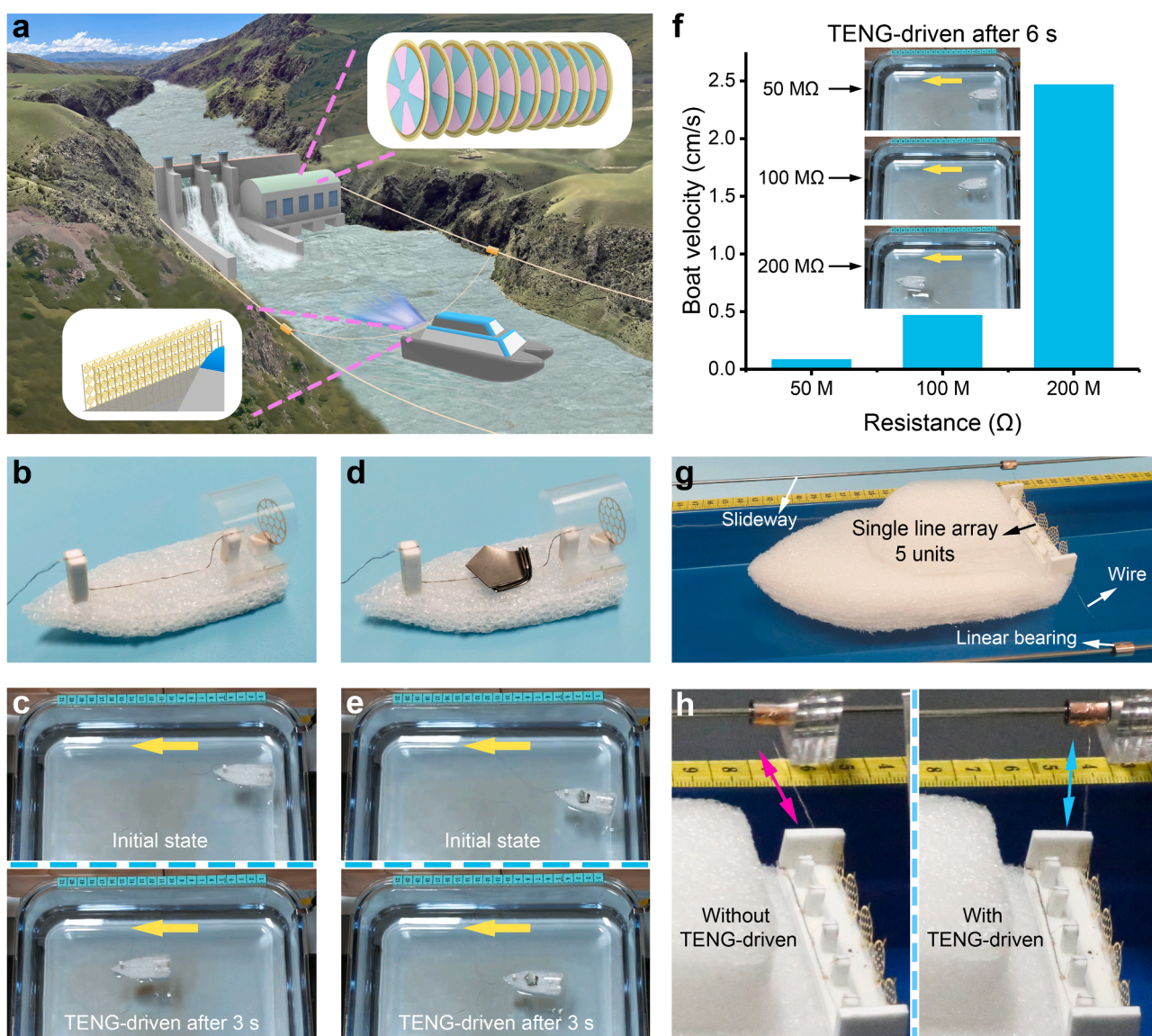


**Fig. 5.** Application demonstrations in water transport. (a) Conceptual schematic of water transport with the TENG-driven EAD propulsion system. (b) Photograph of a foam boat with a EAD thruster. (c) Screenshots of the initial state of the empty boat and its motion state with direct TENG-driven after 3 s (d) Photograph of a foam boat with a EAD thruster and 1.5 g load. (e) Screenshots of the initial state of the loaded boat and its motion state with direct TENG-driven after 3 s (f) Velocity of the empty boat with TENG-driven after 6 s in Method-3 and screenshots of corresponding motion states. (g) Photograph of a larger foam boat with a single line EAD thruster array (5 units) and assistive device. (h) Photographs of motion states of the larger boat without and with direct TENG-driven.

Two metal linear bearings were used as sliders and connected with thrusters by the soft silver wire. It should be noted that it is hard to ignore the friction force between the slider and the slide way. Thus, a motor-driven assistive device was specifically designed to push the slider forward at a little bit slower speed than the boat. As shown in Fig. S21, the assistive device is composed of a cell box with dry cells, a small gear motor, a lead screw, a big acrylic slider with two arms containing two linear bearings and a screw nut, and an acrylic base used to fix all parts. The pink and the blue double-headed arrows drawn in Fig. 5h show significant difference of the silver wire state without and with TENG-driven, indicating that the propulsion system can supply enough thrust force to drive the boat move forward. The detailed demonstrations are shown in Videos S5 and S6.

Supplementary material related to this article can be found online at doi:10.1016/j.nanoen.2022.107558.

Considering that the thruster is light enough, we did some primary exploratory attempts on applications in aviation and space. First, we tried to build a simple micro aircraft and drive it make a successful flight, as conceptually shown in Fig. 6a. A series of two-dimensional

(2D) collector electrodes with different units were designed and prepared, and then they were fabricated into three-dimensional (3D) micro aircrafts by simple bending and sticking (Fig. 6b). The design of multiple thruster units is to show its potential in upgrade for better flying control in the future as the solution adopted by commercial multi-motor unmanned aerial vehicle. The detailed preparation process is illustrated in Fig. S22. To make a good connection with the TENG, an additional plastic stripe was used and part of it was covered with silver paste for conducting electricity. Fig. S23 shows the weight of three types of 3D aircrafts (12.11 mg, 25.61 mg, 34.58 mg). With the direct drive of TENG-25 at the rotation speed of 1000 RPM, these EAD aircrafts can fly successfully in a random state (Video S7-S9). Fig. 6c shows their screenshots of initial states and captured flying attitudes. In addition, the diameter of the EAD thruster unit can be changed to further reduce the weight of the aircraft (Fig. S24).

Supplementary material related to this article can be found online at doi:10.1016/j.jhazmat.2020.124016.

Furthermore, with the help of these two technologies, the astronaut can make a movement control of the spacecraft by utilizing a simple gear

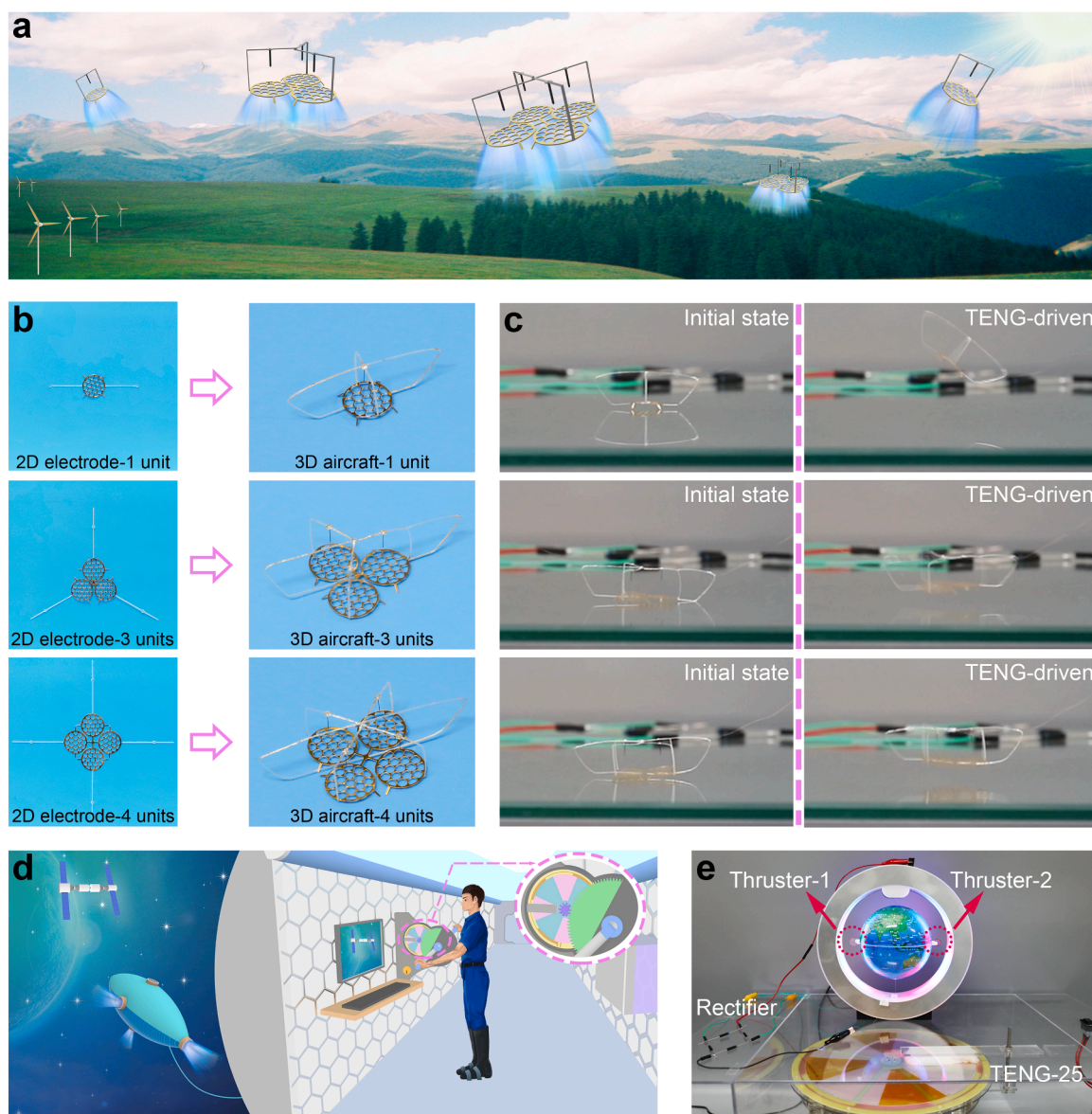


**Fig. 6.** Application demonstrations in aviation and space. (a) Conceptual schematic of different TENG-driven EAD micro aircrafts. (b) Photographs of different 2D collector electrodes and corresponding 3D micro aircrafts. (c) Screenshots of the initial state and the flying state of different micro aircrafts. (d) Conceptual schematic of the TENG-driven EAD spacecraft powered by human mechanical energy. (e) Photograph of a maglev state globe with two TENG-driven EAD thrusters.

mechanical structure with TENGs and multiple thrusters in different directions (Fig. 6d). The spacecraft can be connected with the spaceship by a special composite cable containing conducting wire and gas tube, and the gas can be obtained from the fermentation of organic waste produced by human. Such a system will reduce the energy consumption, and decrease non-essential extravehicular activities, which is a promising way for maintenance of equipment, special rescue, and extravehicular exploration in space. Since it is very hard to have a real space environment, we made a simple simulated zero-gravity condition to investigate the potential of this propulsion system. A maglev globe with a diameter of 110 mm was introduced to create the approximate condition. Two EAD thrusters were stuck on the globe with opposite positions (Fig. 6e). The total weight is as large as 90.8 g (see Fig. S25). Video S10 shows that the maglev globe gradually turned with an increasing speed under the direct drive of TENG-25, indicating an excellent working state and a great application potential in the future.

Supplementary material related to this article can be found online at doi:10.1016/j.nanoen.2022.107558.

#### 4. Conclusions

In conclusion, a simple and easy-fabricated plastic film based light-weight EAD thruster was demonstrated. By utilizing the natural advantage of TENG in high voltage output, they are combined together into a complete propulsion system. Three kinds of methods with different circuits were investigated to realize the effective and controllable drive of the EAD thruster. And the method using a voltage booster circuit and different parallel resistors was recommended. With TENG-driven, the EAD thrusters were used to propel boats moving forward, build multiform 3D micro aircrafts for a successful flight and propel the maglev globe rotating, showing broad application prospects in multiple fields. Although there are lots of technical challenges, the integration of two promising technologies lights a way that could give full play to their strengths, which will be a great help to achieve the goal of carbon neutrality and play a role in more uncharted territories.

#### CRediT authorship contribution statement

**Kai Han:** Conceptualization, Project administration, Investigation, Formal analysis, Validation, Visualization, Writing – original draft, Funding acquisition. **Jianjun Luo:** Investigation, Visualization, Writing – original draft, Funding acquisition. **Jian Chen:** Conceptualization, Investigation, Validation, Writing – original draft. **Yujin Liu:** Investigation. **Jinliang Li:** Investigation. **Zhong Lin Wang:** Supervision, Resources, Writing – review & editing, Funding acquisition. **Wenjie Mai:** Supervision, Resources, Writing – review & editing, Funding acquisition.

#### Declaration of Competing Interest

The authors declare that they have no known competing financial interests or personal relationships that could have appeared to influence the work reported in this paper.

#### Data Availability

Data will be made available on request.

#### Acknowledgements

The research was supported by the National Natural Science Foundation of China (No. 51772135, No. 52172202, No. 22109051, No. 52192610, No. 52002028), the National Key R & D Project from Minister of Science and Technology (No. 2021YFA0202704), the Fundamental Research Funds for the Central Universities (No. 11619103), the Shenzhen Science and Technology Program (JCYJ20200109113606007) and the China Postdoctoral Science

Foundation (No. BX20190324).

#### Author contributions

K.H., J.L. and J.C. contributed equally to this work. Z.L.W. and W.M. supervised the project. K.H. and J.C. conceived the project. K.H. designed the experimental procedures, fabricated the devices, performed the measurements and data analysis. J.C. and K.H. designed the simulation. J.L. and K.H. shot videos of application demonstrations. Y.L. and J.L. helped to prepare the thrusters. K.H. arranged the figures and edited the videos. K.H., J.L., J.C., Z.L.W. and W.M. wrote the manuscript. All authors contributed to the paper.

#### Appendix A. Supporting information

Supplementary data associated with this article can be found in the online version at doi:10.1016/j.nanoen.2022.107558.

#### References

- [1] M. Robinson, A history of the electric wind, *Am. J. Phys.* 30 (1962) 366–372.
- [2] A.P. Chattock, XLIV. On the velocity and mass of the ions in the electric wind in air, *London, Edinburgh, and Dublin Philos. Mag. J. Sci.* 48 (1899) 401–420.
- [3] A.P. Chattock, W.E. Walker, E.H. Dixon, IV. On the specific velocities of ions in the discharge from points, *London, Edinburgh, and Dublin, Philos. Mag. J. Sci.* 1 (1901) 79–98.
- [4] O.M. Stuetzer, Instability of certain electrohydrodynamic systems, *Phys. Fluids* 2 (1959) 642–648.
- [5] O.M. Stuetzer, Ion drag pressure generation, *J. Appl. Phys.* 30 (1959) 984–994.
- [6] M. Robinson, Movement of air in the electric wind of the corona discharge, *Trans. Am. Inst. Electr. Eng. Part I* 80 (1961) 143–150.
- [7] E.A. Christenson, P.S. Moller, Ion-neutral propulsion in atmospheric media, *AIAA J.* 5 (1967) 1768–1773.
- [8] K. Masuyama, S.R.H. Barrett, On the performance of electrohydrodynamic propulsion, *Proc. R. Soc. A* 469 (2013), 20120623.
- [9] C.K. Gilmore, S.R.H. Barrett, Electrohydrodynamic thrust density using positive corona-induced ionic winds for in-atmosphere propulsion, *Proc. R. Soc. A* 471 (2015), 20140912.
- [10] N. Monrolin, F. Flouraboué, O. Praud, Electrohydrodynamic thrust for in-atmosphere propulsion, *AIAA J.* 55 (2017) 4296–4305.
- [11] E. Moreau, Airflow control by non-thermal plasma actuators, *J. Phys. D: Appl. Phys.* 40 (2007) 605–636.
- [12] P.H.G. Allen, T.G. Karayiannis, Electrohydrodynamic enhancement of heat transfer and fluid flow, *Heat. Recovery Syst. CHP* 15 (1995) 389–423.
- [13] I.Y. Chen, M.-Z. Guo, K.-S. Yang, C.-C. Wang, Enhanced cooling for LED lighting using ionic wind, *Int. J. Heat. Mass Transf.* 57 (2013) 285–291.
- [14] A. Singh, V. Orsat, V. Raghavan, A comprehensive review on electrohydrodynamic drying and high-voltage electric field in the context of food and bioprocessing, *Dry. Technol.* 30 (2012) 1812–1820.
- [15] J.-L. Naudin, The lifter "maximus" [": 250 g weight. (<http://jnaudin.free.fr./lifters/maximus2/>), 2003 (Accessed 21 December 2016).
- [16] D.S. Drew, K.S.J. Pister, Geometric optimization of microfabricated silicon electrodes for corona discharge-based electrohydrodynamic thrusters, *Micromachines* 8 (2017) 141.
- [17] D.S. Drew, N.O. Lambert, C.B. Schindler, K.S.J. Pister, Toward controlled flight of the ionocraft: a flying microrobot using electrohydrodynamic thrust with onboard sensing and no moving parts, *IEEE Robot. Autom. Lett.* 3 (2018) 2807–2813.
- [18] H. Xu, Y. He, K.L. Strobel, C.K. Gilmore, S.P. Kelley, C.C. Hennick, T. Sebastian, M. R. Woolston, D.J. Perreault, S.R.H. Barrett, Flight of an aeroplane with solid-state propulsion, *Nature* 563 (2018) 532–535.
- [19] F.-R. Fan, Z.-Q. Tian, Z.L. Wang, Flexible triboelectric generator!, *Nano Energy* 1 (2012) 328–334.
- [20] Z.L. Wang, On Maxwell's displacement current for energy and sensors: the origin of nanogenerators, *Mater. Today* 20 (2017) 74–82.
- [21] Z.L. Wang, On the expanded Maxwell's equations for moving charged media system – general theory, mathematical solutions and applications in TENG, *Mater. Today* 52 (2022) 348–363.
- [22] Z.L. Wang, Triboelectric nanogenerators as new energy technology for self-powered systems and as active mechanical and chemical sensors, *ACS Nano* 7 (2013) 9533–9557.
- [23] X.-S. Zhang, M. Han, B. Kim, J.-F. Bao, J. Brugger, H. Zhang, All-in-one self-powered flexible microsystems based on triboelectric nanogenerators, *Nano Energy* 47 (2018) 410–426.
- [24] C. Wu, A.C. Wang, W. Ding, H. Guo, Z.L. Wang, Triboelectric nanogenerator: a foundation of the energy for the new era, *Adv. Energy Mater.* 9 (2019), 1802906.
- [25] J. Luo, Z. Wang, L. Xu, A.C. Wang, K. Han, T. Jiang, Q. Lai, Y. Bai, W. Tang, F. R. Fan, Z.L. Wang, Flexible and durable wood-based triboelectric nanogenerators for self-powered sensing in athletic big data analytics, *Nat. Commun.* 10 (2019) 5147.

- [26] K. Han, J. Luo, Y. Feng, L. Xu, W. Tang, Z.L. Wang, Self-powered electrocatalytic ammonia synthesis directly from air as driven by dual triboelectric nanogenerators, *Energy Environ. Sci.* 13 (2020) 2450–2458.
- [27] W. He, W. Liu, J. Chen, Z. Wang, Y. Liu, X. Pu, H. Yang, Q. Tang, H. Yang, H. Guo, C. Hu, Boosting output performance of sliding mode triboelectric nanogenerator by charge space-accumulation effect, *Nat. Commun.* 11 (2020) 4277.
- [28] H. Feng, Y. Bai, L. Qiao, Z. Li, E. Wang, S. Chao, X. Qu, Y. Cao, Z. Liu, X. Han, R. Luo, Y. Shan, Z. Li, An ultra-simple charge supplementary strategy for high performance rotary triboelectric nanogenerators, *Small* 17 (2021), 2101430.
- [29] Z. Wang, W. Liu, W. He, H. Guo, L. Long, Y. Xi, X. Wang, A. Liu, C. Hu, Ultrahigh electricity generation from low-frequency mechanical energy by efficient energy management, *Joule* 5 (2021) 441–455.
- [30] Y. Pang, Y. Cao, M. Derakhshani, Y. Fang, Z.L. Wang, C. Cao, Hybrid energy harvesting systems based on triboelectric nanogenerators, *Matter* 4 (2021) 116–143.
- [31] C. Shan, W. He, H. Wu, S. Fu, Q. Tang, Z. Wang, Y. Du, J. Wang, H. Guo, C. Hu, A high-performance bidirectional direct current TENG by triboelectrification of two dielectrics and local corona discharge, *Adv. Energy Mater.* (2022), 2200963.
- [32] J. Nie, Z. Ren, J. Shao, C. Deng, L. Xu, X. Chen, M. Li, Z.L. Wang, Self-powered microfluidic transport system based on triboelectric nanogenerator and electrowetting technique, *ACS Nano* 12 (2018) 1491–1499.
- [33] Y. Zi, C. Wu, W. Ding, X. Wang, Y. Dai, J. Cheng, J. Wang, Z. Wang, Z.L. Wang, Field emission of electrons powered by a triboelectric nanogenerator, *Adv. Funct. Mater.* 28 (2018), 1800610.
- [34] A.Y. Li, Y.L. Zi, H.Y. Guo, Z.L. Wang, F.M. Fernandez, Triboelectric nanogenerators for sensitive nano-coulomb molecular mass spectrometry, *Nat. Nanotechnol.* 12 (2017) 481–487.
- [35] J. Cheng, W. Ding, Y. Zi, Y. Lu, L. Ji, F. Liu, C. Wu, Z.L. Wang, Triboelectric microplasma powered by mechanical stimuli, *Nat. Commun.* 9 (2018) 3733.
- [36] M.-C. Wong, W. Xu, J. Hao, Microplasma-discharge-based nitrogen fixation driven by triboelectric nanogenerator toward self-powered mechano-nitrogenous fertilizer supplier, *Adv. Funct. Mater.* 29 (2019), 1904090.
- [37] K. Han, J. Luo, J. Chen, B. Chen, L. Xu, Y. Feng, W. Tang, Z.L. Wang, Self-powered ammonia synthesis under ambient conditions via  $N_2$  discharge driven by Tesla turbine triboelectric nanogenerators, *Microsyst. Nanoeng.* 7 (2021) 7.
- [38] H. Guo, J. Chen, L. Wang, A.C. Wang, Y. Li, C. An, J.-H. He, C. Hu, V.K.S. Hsiao, Z. L. Wang, A highly efficient triboelectric negative air ion generator, *Nat. Sustain.* 4 (2021) 147–153.
- [39] Y. Bai, S. Chen, H. Wang, E. Wang, X. Kong, Y. Gai, X. Qu, Q. Li, S. Xue, P. Guo, R. Wang, H. Feng, Z. Li, Chemical warfare agents decontamination via air microplasma excited by a triboelectric nanogenerator, *Nano Energy* 95 (2022), 106992.
- [40] S. Niu, Z.L. Wang, Theoretical systems of triboelectric nanogenerators, *Nano Energy* 14 (2015) 161–192.
- [41] P. Chen, J. An, R. Cheng, S. Shu, A. Berbille, T. Jiang, Z.L. Wang, Rationally segmented triboelectric nanogenerator with a constant direct-current output and low crest factor, *Energy Environ. Sci.* 14 (2021) 4523–4532.



**Dr. Jian Chen** received his B.S. degree in Central South University in 2014, and his Ph.D. degree in Condensed Matter Physics from University of Chinese Academy of Sciences in 2019. He joined Nanyang Technological University as a postdoctoral fellow from 2019 to 2022. His research interests include triboelectric nanogenerators, self-powered systems and soft robot.



**Yujin Liu** received his B.S. degree in Electronic Information Engineering (2016) from Wuyi University and M.S. degree in Condensed Matter Physics from Jinan University (2019). He is currently a Ph.D. candidate in Optical Engineering at Jinan University. His main research interest is photodetector and imaging.



**Dr. Jinliang Li** received his B.S. degree in Electronic Science and Technology (2012) from South China University of Technology (SCUT) and his Ph. D degree in Physics (2017) from East China Normal University (ECNU). He is now an Associate Professor in Jinan University (JNU). His main research interests are alkalis-ion batteries.



**Prof. Zhong Lin Wang** received his Ph.D. degree from Arizona State University in physics. He now is the Hightower Chair in Materials Science and Engineering, Regents' Professor at Georgia Tech, the chief scientist and director of the Beijing Institute of Nanoenergy and Nanosystems, Chinese Academy of Sciences. Prof. Wang has made original and innovative contributions to the synthesis, discovery, characterization and understanding of fundamental physical properties of oxide nanobelts and nanowires, as well as applications of nanowires in energy sciences, electronics, optoelectronics and biological science. His discovery and breakthroughs in developing nanogenerators establish the principle and technological road map for harvesting mechanical energy from environmental and biological systems for powering personal electronics. His research on self-powered nanosystems has inspired the worldwide efforts in academia and industry for studying energy for micro-nano-systems, which is now a distinct disciplinary in energy research and future sensor networks. He coined and pioneered the fields of piezotronics and piezophotonics by introducing piezoelectric potential gated charge transport process in fabricating new electronic and optoelectronic devices.



**Prof. Wenjie Mai** received his B.S. degree in Physics (2002) from Peking University (PKU) and his Ph.D. degree in Materials Science and Engineering (2009) from the Georgia Institute of Technology (GIT). He is now a Professor in Jinan University (JNU). His main research interest includes energy conversion, harvesting and storage devices, such as supercapacitors, dye-sensitized solar cells, nanogenerators, and photoelectrochemical water splitting.



**Dr. Kai Han** received his B.E. degree in Macromolecular Materials and Engineering from Qingdao University in 2012, M.E. degree in Applied Chemistry from Shanghai University in 2015, and Ph.D. degree in Condensed Matter Physics from University of Chinese Academy of Sciences in 2020. He is now a postdoctoral fellow in Jinan University and a visiting fellow in Beijing Institute of Nanoenergy and Nanosystems, Chinese Academy of Sciences. His research interests include triboelectric nanogenerators, self-powered electrochemistry and systems.



**Dr. Jianjun Luo** received his B.S. degree in Applied Chemistry from Jinan University in 2013, and his Ph.D. degree in Condensed Matter Physics from University of Chinese Academy of Sciences in 2018. After graduation, he worked in Beijing Institute of Nanoenergy and Nanosystems as a postdoctoral research fellow. He is now an associate professor in Beijing Institute of Nanoenergy and Nanosystems, Chinese Academy of Sciences. His research interests include triboelectric nanogenerators, self-powered systems and supercapacitors.